

Indexed by

Scopus<sup>®</sup>

## CREATION OF IMAGE MODELS FOR INSPECTING DEFECTS IN COMMERCIAL DRIED FISH FLOSS

DOAJ  
DIRECTORY OF  
OPEN ACCESS  
JOURNALS**Hong-Dar Lin**

Chaoyang University of Technology, College of Science and Engineering, Department of Industrial Engineering and Management, Taichung, Taiwan

**Chang-Yi Lin**

Chaoyang University of Technology, College of Science and Engineering, Department of Industrial Engineering and Management, Taichung, Taiwan

**Ching-Hsiang Lin**

National Kaohsiung University of Science and Technology, Business Intelligence School, Department of Accounting and Information Systems, Kaohsiung, Taiwan

 Crossref ROAD KoBSON

**Key words:** fish floss, computer vision, visual defect, curvelet transform

doi:10.5937/jaes18-27185

 SCINDEKS  
Srpski citatni indeks**Cite article:**

Lin, D. H., Lin, Y. C., & Lin C. H.. [2020]. Creation of image models for inspecting defects in commercial dried fish floss. *Journal of Applied Engineering Science*, 18(3), 393 - 402.

 Google

**Online access** of full paper is available at: [www.engineeringscience.rs/browse-issues](http://www.engineeringscience.rs/browse-issues)

## CREATION OF IMAGE MODELS FOR INSPECTING DEFECTS IN COMMERCIAL DRIED FISH FLOSS

Hong-Dar Lin<sup>1\*</sup>, Chang-Yi Lin<sup>1</sup>, Ching-Hsiang Lin<sup>2</sup>

<sup>1</sup>Chaoyang University of Technology, College of Science and Engineering, Department of Industrial Engineering and Management, Taichung, Taiwan

<sup>2</sup>National Kaohsiung University of Science and Technology, Business Intelligence School, Department of Accounting and Information Systems, Kaohsiung, Taiwan

Fish floss is a chopped finely or mashed fish meat boiled in seasonings, then stir fry until the fish meat is arid and pulverous. In the making of commercial fish flosses, defect inspection is conducted by expertise inspectors using their feeling of contact and sight which could cause misjudgments. When consumers eat fish floss with defects, it may cause harm to the health of consumers. Therefore, this study proposes an automated defect detection method and develop an optical inspection system for commercial dried fish floss. The proposed method applies the curvelet transform with low-pass energy filtering to remove the random patterns of background and delete the angle direction of background texture. The approximated and partial detailed components regarding defects and uniform background are preserved in the low and medium frequency bands. In the reconstructed image, the background random texture is attenuated and the defect areas are enhanced. Finally, the restored image can be easily segmented by an estimated threshold value into two categories namely dark defects, and white background. The experimental results show that the proposed method well balances the trade-off between the recall rate (82.11%) and precision rate (87.62%), and reaches an F-score of 84.78%, outperforming the traditional defect detection techniques in inspection of dried fish floss.

*Key words:* fish floss, computer vision, visual defect, curvelet transform

### INTRODUCTION

Both fish and fish related products are two common foods in our daily lives. Since fish products have highly economic value, the main form of direct consumption of raw fish, cooked fish, processed products (such as preserved fish, canned fish, fish floss, etc.) is fairly extensive. Figure 1 shows three common processed fish products, pickled fish, dried salted fish, and fish floss. Fish floss is a processed product that produced from fresh fish by means of the process of grinding, frying, and adding food spices and additives to gain a flavorful taste [1]. It comes from a chopped finely or mashed fish meat boiled in seasonings, then stir fry until the fish meat is arid and pulverous. This fish floss is good to be eaten with hot steam rice, as topping for porridge, or you can even eat it with slices of white bread, or to be made as fish floss roll.

Generally, the procedures of dealing with fish into floss

comprises some steps, which are the collecting and selecting raw materials, separating fish meat, making seasonings, boiling, cooking and packaging the produced fish floss [2]. Some defects in fish floss can result from incomplete separation and cleaning of fish meat, unsuitable temperature controls of ovens, and inappropriate stir-fry operations during the production. Figure 2 illustrates four common defect types in fish floss, clumping floss, burnt floss, fish bones, fish tendons. In the making of commercial fish flosses, defect detection is conducted by expertise inspectors using their feeling of contact and sight which could cause misjudgments. Figure 3 shows the current manual inspection of commercial fish floss in production lines. Mistaken judgements are merely made since sensors' eye exhaustion and subjectiveness. When consumers eat fish floss with defects, it may cause harm to the health of consumers. Therefore, this study proposes an automated defect detection method and develop an optical inspection system for commercial

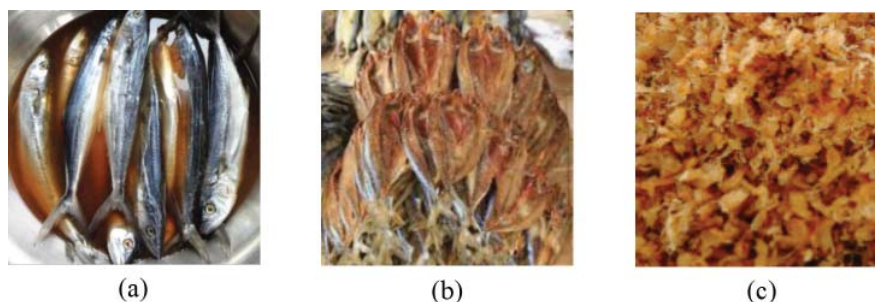


Figure 1: Three common processed fish products: (a) pickled fish; (b) dried salted fish; (c) fish floss

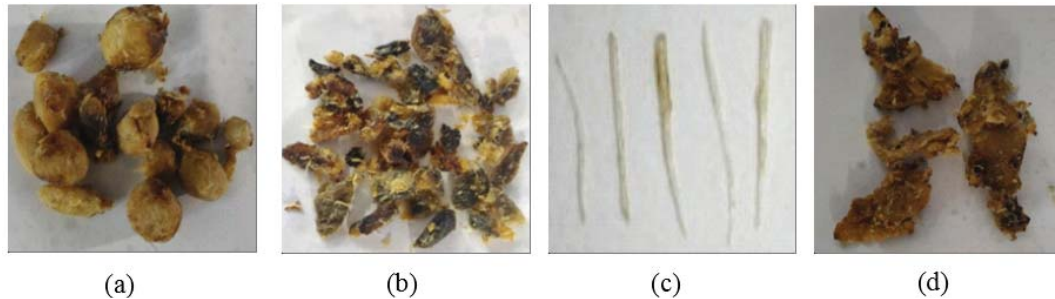


Figure 2: Four common types of visual defects in fish floss: (a) clumping floss; (b) burnt floss; (c) fish bones; (d) fish tendons

dried fish floss. The four common defect types in fish floss will be the targets to be investigated by the system. The inspection of fish bone defects is the major concern in this study.

The fried fish floss samples need be spread out evenly on a platform before capturing images by using a vision system. Figure 4 shows three fish floss images, one normal image without fish bone, two defective images with two and four fish bones. The goal of this work is to explore the use of an optical system to detect the near-surface defects in fish floss samples. Difficulties exist in correctly inspecting defects of fish floss by vision systems since when fish floss images are being acquired, the scope of a defect could dilate, reduce or unexpectedly vanish owing to irregular lighting of the surrounding, texture structures and bumpy surfaces of the products, and so on. Since the textured fish floss has the appearance of random patterns, those evident textures make the fault identification work with more difficulty when visible faults are inlaid on the bumpy exteriors with random textures. We thereby propose a curvelet transform based approach to defeat these troubles of automated visual defect identification of fish floss.



Figure 3: Traditional human inspection using hands to remove defects in fish floss products

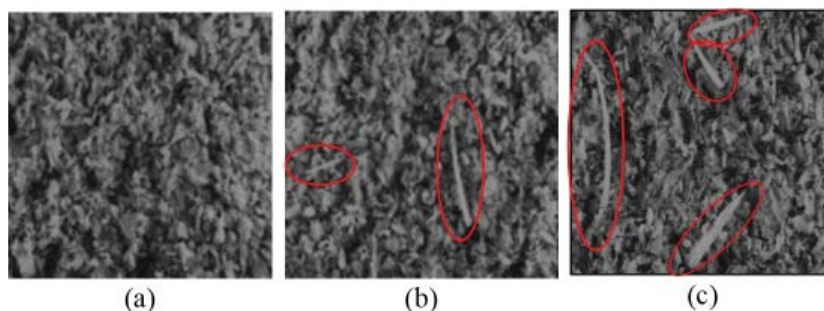


Figure 4: Fish floss images: (a) without fish bone; (b) with two fish bones; (c) with four fish bones

The remainder of the article is organized as follows: Firstly, we review the articles on current techniques of image processing for quality inspection of food products. Secondly, we describe the proposed curvelet transform approach for detecting visual defects in fish floss. Thirdly, we execute the trials and assess the manifestation of the suggested approach with traditional techniques. Finally, we conclude the contributions and indicate the further directions.

### LITERATURE REVIEW

Machine vision offers an option for an automatic, non-contact and cost-effective technique to achieve the requirement for precise, rapid and impartial quality inspection in many industrial applications [3-5]. The inspection method based on image analysis and pattern recognition techniques has created various applications in the food industry. Gowen et al. [6] implemented a hybrid approach combining principal components analysis (PCA) with linear discriminant analysis to identify freeze damages on mushrooms using hyperspectral imaging. Huang et al. [7] developed a multispectral imaging device based on chosen valid wavelengths employing a segmented PCA method for real time detection of bruises on apples. Khoje et al. [8] implemented a skin flaw detection system for quality rating of guava and lemon fruits utilizing support vector machine (SVM) classifier based on frequency features in curvelet transform. Chen and Qin [9] developed a segmentation technique for the beef-marbling image using thresholding to make scores in a beef quality grading system. Brosnan and Sun [10] presented the notable components of a machine vision system and reviewed the most recent applications of quality inspection in food industry.

Some studies investigate the quality inspection of fish

related products. Since fish bones are some of the most regularly gulped extraneous objects happened in foods, fishbone detection is the main task in quality inspection of fish products. Andersen [11] proposed a generation method of fish fillet processing lines for whitefish to verify the absence of bones through X-ray image analysis. Han and Shi [12] developed a method combining particle swarm clustering and morphological operations with high effectiveness in fish bone detection for radiographic images. Thielemann et al. [13] presented an approach using texture analysis of surface image to forecast the locations where fish bones could be existent in the fish fillet. Sivertsen et al. [14] described the use of a ridge detection method to find the centerline on cod fillets for quality inspection. Mery et al. [15] proposed an X-ray computer vision method to inspect fish bones in fish fillets of salmon and trout. Rerkratn and Kaewpoonsuk [16] developed a system for quality assessment of fish fillet employing K-means clustering and thresholding skills. They evaluated the quality of fish fillet is dependent on percent of fish fillet and fishbone region. From the above reviews of literatures, almost all of the proposed fishbone detection methods were developed for fish fillets [11-16] and through radiographic images [11-12,15]. Those developed systems are expensive for the X-ray related devices. In addition, these researches do not inspect faults with attributes of small fish bones on bumpy exteriors of fish floss products. Accordingly, this study applies curvelet transform filtering approach to defect detection on bumpy surfaces of fish floss and implements a low-cost vision system for fishbone inspection in fish floss products.

The curvelet transform was invented to make better the drawbacks of usual two-dimensional (2-D) discrete wavelet transforms. Curvelets constitute a valid model thinking over a multiscale time-frequency local partition as well as utilizing the direction of geometric features. The curvelet transform offers a nearly optimal sparse expression of objects in 2-D cases. Its beneficial quickness and simpleness also facilitate the wide implementations of curvelets in many scientific and engineering fields. Boubchir and Fadili [17] presented a statistical examination of the components' dependencies of the images covering position, scale and direction in the curvelet domain for applications of image restoration. Jiang and Zhao [18] developed a superior curvelet method to reach better denoising result and have the extensive serviceableness for remote sensing images. Zhang, Li, and Li [19] proposed a curvelet transform based method to improve Canny edge operator for edge detection in tire laser shearography images. Some studies proposed mixed methods based on curvelet transform for classifications, such as combining with morphological feature extraction method to characterize non-stochastic surfaces for metrology [20], fusing with Kirsch's templates to extract retinal blood vessels for detection of diabetes at early stages [21], integrating with PCA method to extract features from still images for face recognition [22].

## MATERIALS AND METHODS

This research presents a curvelet transform based low-pass filtering approach to detect defects on surfaces of evenly-spread fish floss. Five steps are developed to perform the process of defect inspection. Firstly, image preprocessing is to resize testing images to be exactly the specified size 256 x 256 pixels for avoiding longer processing waiting time related with further image processing analysis. Secondly, the resized spatial domain image is converted to CT domain based on the specified CT parameters, scale and angle. Thirdly, by selecting a proper scope for filtering in frequency domain, the low-frequency parts more than the scope are retained and the remainders are given to zero for reconstructing the image surface. There is detailed message regarding defects and uniform background in the preserved low-frequency elements than those in the high-frequency elements. Fourthly, the filtered frequency image is executed by the inverse curvelet transform to make a reconstructed image. Thus, a defect-enhanced image could be reconstructed from the frequency domain for contrasting with the initial image. Fifthly, the rebuilt image can be simply classified into two categories (dark defects and white background) by applying a statistical interval estimation theory and several properties of the recognized defects are extracted. Therefore, the visual defects on the bumpy surfaces with random texture of fish floss can be accurately identified and located by the proposed approach. The flow chart of the proposed methodology is shown in Figure 5.

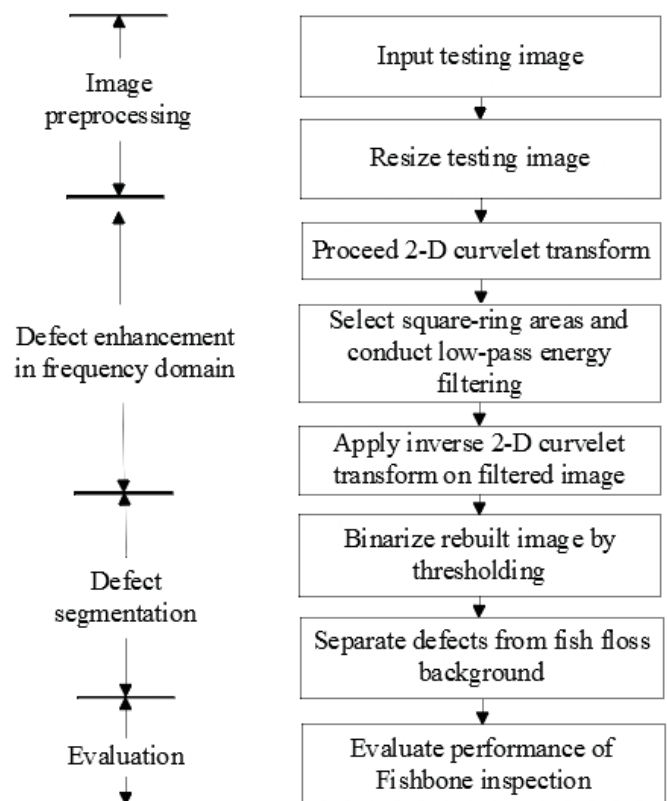


Figure 5: Proposed methodology for defect detection in dried fish floss

### Image Modeling & Analysis

A model being a description of a system using different concepts can help to explain a system and to study the effects of different components, and to make predictions of the system behavior [23]. Modeling is the process of developing a model. Salau and Jain developed the materials and methods employed for computational modeling and experimental analysis for the diagnosis of cell survival/death for AKT protein [24]. This study creates mathematical models based on the image characteristic features in curvelet domain to find extensive practical applications in vision systems for defect detection in dried fish floss. Curvelet transform is one kind of multiscale directional transformations involving multi-layer decompositions and reconstructions. It was invented by Candes and Donoho in 2000 [25] applying ridgelet analysis to radon transform. The curvelet transform is distinctive in its computation as it calculates coefficients at every scale, orientation and position. For discrete image processing, the feed in image is in the format of a Cartesian array; therefore, the rotation alters to shear and the computation arises in a pseudo-polar coordinate plan [26]. The curvelet transform is an expansion of the wavelet transform revealing superior directionality and rebuilding. Candes et al. suggested a revised version of curvelet transform, called fast discrete curvelet transform (FDCT) being quicker, easier and reduced redundant than the original ridgelet transform [27].

The FDCT in this study is executed employing a wrapping-based method. The choice of wrapping-based method is made due to simplicity of execution and lesser processing time. The wrapping-based FDCT is a multiscale pyramid including distinct orientations and positions in frequency domain. It employs merits of fast Fourier transform (FFT) in Fourier spectral domain. In the process of FFT, the image and curvelet with a specified scale and direction are converted into the Fourier domain. After transformation process, we obtain a set of curvelet coefficients through utilizing reverse FFT to the spectral product. This set includes curvelet coefficients in rising sequence of the scales and directions.

FDCT utilizing frequency wrapping is employed to the transformed image to gain curvelet coefficients through computing image orientation from distinct angles. The stages of FDCT approach based on wrapping applied to this study are summarized as the following [27]:

**Step 1.** A testing image  $f(x, y)$  with  $N \times N$  size is converted into the frequency domain by forward 2-D FFT,

$$F[u, v] = \frac{1}{N^2} \sum_{x=0}^{N-1} \sum_{y=0}^{N-1} f(x, y) \exp[-j \cdot 2\pi(ux/N + vy/N)] \quad (1)$$

**Step 2.** The transformed image  $F[u, v]$  is then multiplied by a set of discrete localizing window functions  $\tilde{U}_{j,l}$ . For every scale  $j$  and orientation  $l$ , it forms the product  $\tilde{U}_{j,l}[u,v] F[u, v]$ . The shape of these windows are defined in accordance with the conditions of the ideal curvelet

transform.

**Step 3.** The products on these districts are wrapped around the origin into rectangular shape,

$$\tilde{F}_{j,l}[u, v] = W(\tilde{U}_{j,l} F)[u, v] \quad (2)$$

**Step 4.** Utilize the inverse 2-D FFT to each wrapped coefficients,

$$f(x, y) = \sum_{u=0}^{N-1} \sum_{v=0}^{N-1} \tilde{F}_{j,l}[u, v] \exp[j \cdot 2\pi(ux/N + vy/N)] \quad (3)$$

**Step 5.** Gather the discrete curvelet coefficients  $c^D(j, l, k)$  from the inversed FFT image,  $f'(x, y)$  where  $j, l, k$  represent the scale, orientation, and position parameters,

$$c^D(j, l, k) = \sum_{0 \leq x, y < n} f(x, y) \cdot \phi_{j,l,k}^D[x, y] \quad (4)$$

Each  $c^D(j, l, k)$  represents a discrete curvelet waveform.

These coefficients are filtered out adopting low-passing filtering regulation which chooses the scope of square-ring bands. The filtered coefficients are obtained after the low-passing filtering procedure. The rebuilt image is gained by employing inverse FDCT on the filtered coefficients.

### Feature Extraction

Feature extraction is a skill used for extracting relevant information from an image for further classification. Salau and Jain [28] conducted a survey of the existing techniques, types and applications of feature extraction used in recent times. Curvelet transform is multiscale geometrical transform where units are indexed by their position, scale and orientation. In feature extraction stage, the images are decomposed into its approximate and detailed components using two levels of curvelet transform. These subimages greatly reduces the dimensionality of the original image. Thereafter, only the approximate components are selected to perform further computations, as they account for maximum variance [20, 29]. Thus, a representative and efficient feature set is produced.

Curvelet transform can span the whole frequency space at different scales and directions taking lesser coefficients for a specified exactness of reconstruction. After decomposition of a discrete image applying curvelet transform based on wrapping method, low, medium and high frequency components of the image at each scale are gained. The low-frequency coefficients, called approximated components, are abundant in information regarding background details of an image as well as the medium- and high-frequency coefficients, called detailed components, convey details mostly regarding the edges existing in an image. Figure 6 displays a testing image with size 256 x 256 is performed 1 to 5 decomposition levels of curvelet transformations. The figures show the curvelet coefficients at various scales in 1 to 5 decompo-

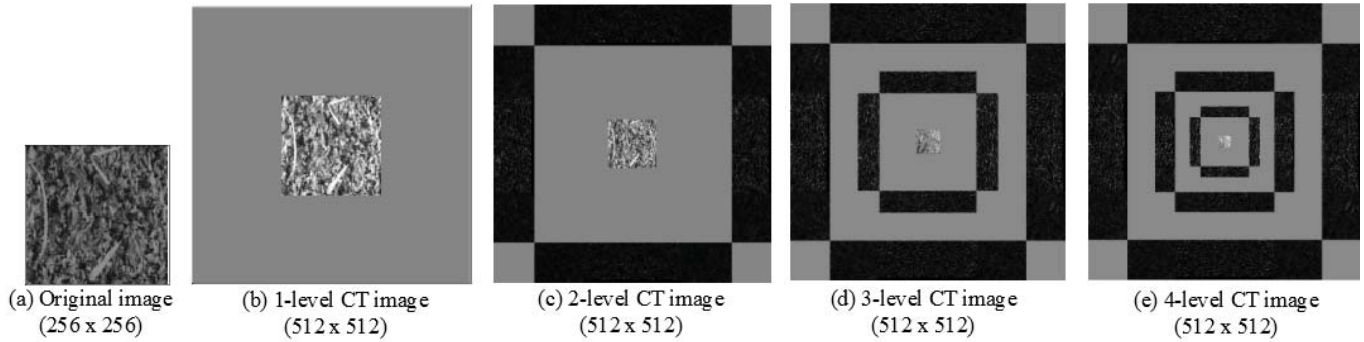


Figure 6: A testing image with size 256 x 256 is performed 1 to 5 decomposition levels of curvelet transformations

sition levels. The central part is the approximated components with low-frequency coefficients, meanwhile, the multiple square-ring bands (marked in black) are the detailed components with high-frequency coefficients. The higher the decomposition levels of curvelet transform are conducted, the larger the band-widths of the square-ring bands are obtained. For each band, it is further partitioned into some districts with distinct polar angles. The locations of energy partitions at different bands could describe the relationship between the detailed components and filtering angles.

**Curvelet Filtering Operation**

To further investigate the filtering effect on the images with random texture, the fish floss images are conducted the curvelet band-pass filterings with various angles retained. Figure 7 depicts the results in the operations of the band-pass filtering by retaining different angles in curvelet domains. The up-row images are the filtered curvelet domain images with red areas removed and black areas retained in the detailed components. The middle-row images are the rebuilt filtered images. The random textures on background are significantly attenuated and become more smooth. The bottom-row images

are the resulting binary images indicating the detection results. Some results reveal large missing defect and many false alarm areas. Different retaining angles of the curvelet band-pass filterings significantly influence the detection results.

After the proper region is determined, the frequency filtering process can correctly recognize the high frequency zones of random textures and these frequency components are set to zero in curvelet domain. Next, we take inverse FFT on the filtered frequency image to convert back to time domain for defect separation. In this work, we plan to remove many random textures in the rebuilt image by selecting a suitable area in the detailed components for the zero-value substitute. Because random textures may represent high power spectrum, rebuilding the detailed components with stress region from those of the ordinary textures will erase almost all random textures in an initial image, and preserve exclusively fractional defects in a rebuilt image. The random textures will cause a approximately consistent intensity, while the fractional defects will generate distinct intensities in the rebuilt image.

The filtered rebuilt image has roughly consistent gray levels for pixels classified to homologous background

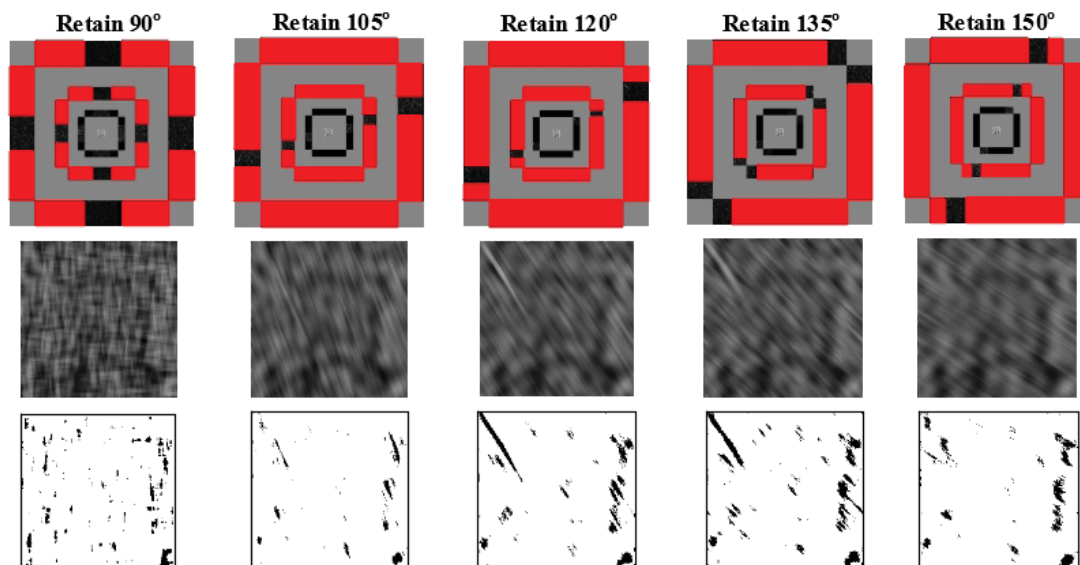


Figure 7: Results in the operations of band-pass filtering by retaining different angles in curvelet domains

zones, but it also produces notably distinct gray levels for pixels classified to nonhomologous defect districts. The intensity changes in homologous districts could be very little, while the intensity changes in nonhomologous regions could be big contrast to the whole rebuilt image. Thence, this study can determine a threshold for distinguishing defects from fish floss area in the reconstructed image. The reconstructed image will be roughly a consistent gray level image if a fish floss product without bones is tested. The upper limit  $T_U$  for gray level changes in the rebuilt image is expressed by  $T_U = \mu + N\sigma$ , where  $\mu$  and  $\sigma$  are the average and standard deviation of the intensities of the rebuilt image  $f(x, y)$ ,  $N$  is a controlled parameter decided by experiments. The binary defect image  $B(x, y)$  for defect segmentation is:

$$B(x, y) = \begin{cases} 255 & , \text{ if } f'(x, y) \leq (\mu + N\sigma) \\ 0 & , \text{ otherwise.} \end{cases} \quad (5)$$

If a pixel with the intensity is less than the upper limit  $T_U$ , the pixel is categorized as a homologous element. On the contrary, it is categorized as a defect element. When the defect sizes to be detected are usually very little contrast to the whole appearance image, the  $\mu$  and  $\sigma$  can be counted straight from the reconstructed image of an initial image to tolerate the illumination variations in the examination circumstance. Figure 8 shows the results in operations of image rebuilt and defect separation. Most of the surface textures are removed in the rebuilt filtered image and the defect is clearly identified meanwhile some false alarms are also made.

## EXPERIMENTS AND DISCUSSION

### Experimental Setup

This study uses the curvelet transform based low-pass filtering approach to develop an automatic optical inspection system for quality assessment of fish floss. The developed inspection system includes hardware for acquiring image data and software for implementing the detection algorithms on the acquired data. To intensify the clearness of object surfaces and defects in fish floss products in the phase of image capture, this study utilizes the subsequent devices in the implemented inspection environment: a lighting frame with two incandescent light bulbs, a black and white charge-coupled device camera with 500M, a lens with 1 to 10 amplifications of changeable focal lengths 13-130 mm, and an electronically con-

trolled table. The vision system adopts two sided lighting with proper angle control and the capture area is 130.2 x 97.6 mm<sup>2</sup> for each shot. Figure 9 illustrates the schematic diagram with specifications and the hardware setup of the vision system. Assessments are performed on 150 real fish floss samples (50 images without defects and 100 images with defects) to appraise the representation of the proposed method. Every image has a size of 256 x 256 pixels with an intensity of 8 bits. The defect identification algorithm is edited in MATLAB language and executed on the R2010b version on a computer (INTEL P4-2.8GHz 512MB RAM).

To mathematically examine the representation of the recommended technique, we differ the outcomes of our appraisals from those offered by practical examiners (ground truth). The expression guides,  $(1-\alpha)$  and  $(1-\beta)$ , are used to express proper inspection assessments; the larger the two guides, the more precise the inspection outcomes. False alarm mistake ( $\alpha$ , regarding fish floss districts as defects) divides the regions of fish floss districts inspected as defects by the regions of actual fish floss districts to gain the mistake. Missing alarm mistake ( $\beta$ , unsucceeding to alarm actual defects) divides the regions of uninspected actual defects by the regions of all actual defects to obtain the mistake. For the both mistakes, the lower the guide values, the better the detection outcomes [30].

To make the user's interaction design, visual design, and information architecture as simple and efficient as possible in software part of the developed inspection system, Figure 10 illustrates a design of human-computer interaction for defect detection. The interaction design describes the consequences and differentiations performed by the suggested method of curvelet transformation in diverse phases for detecting defects in fish floss surfaces. The image (1) is an acquired image from a portion of a trial fish floss. The image (2) is a transformed image through the curvelet transform applied to the original image. The image (3) presents a filtered image after the low-pass energy filtering is executed. The image (4) is a rebuilt image after some high-frequency coefficients specified by the assigned scope were recovered in curvelet domain and then the inverse FFT is taken. After performing image binarization by using statistical interval estimation, the image (5) reveals that the fish bones on the fish floss are exactly identified in a binary image, regardless of the uneven exteriors and light changes.

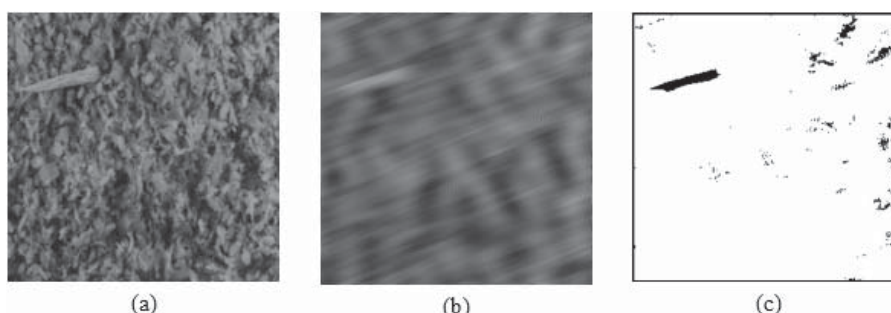


Figure 8: Processed images: (a) original image; (b) rebuilt filtered image; (c) binary resulting image

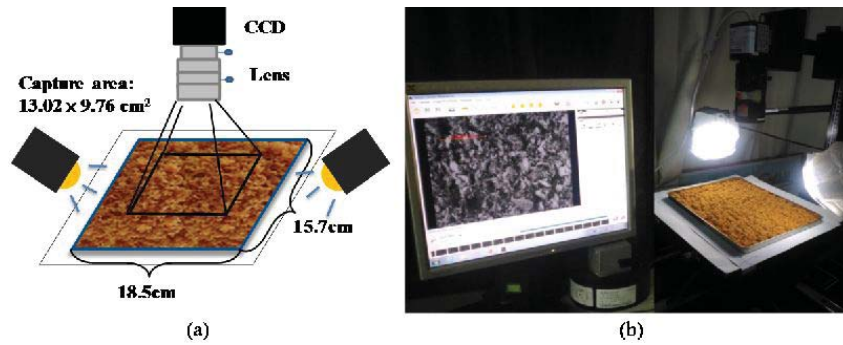


Figure 9: Configuration of capturing fish floss images: (a) schematic diagram with specifications; (b) hardware setup of the vision system

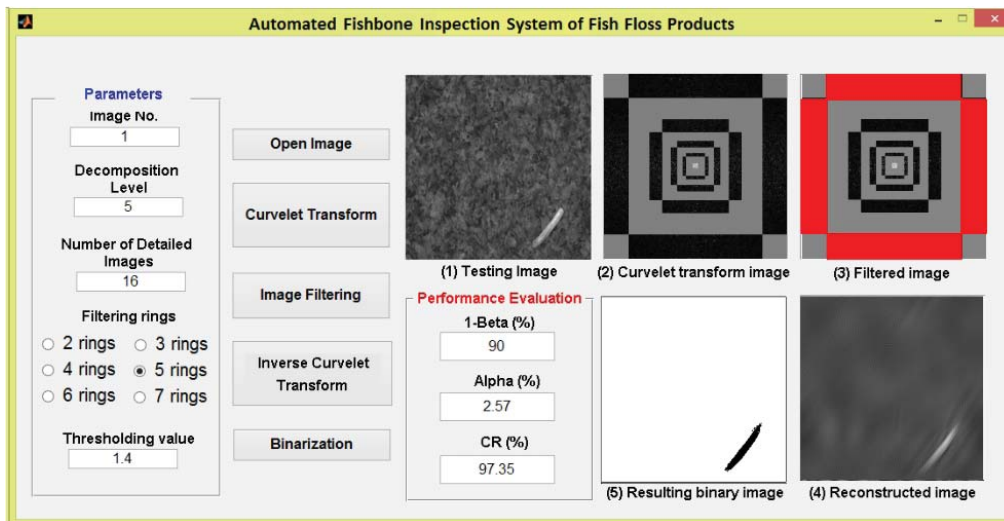


Figure 10: Layout of human-computer interaction for the suggested defect inspection system

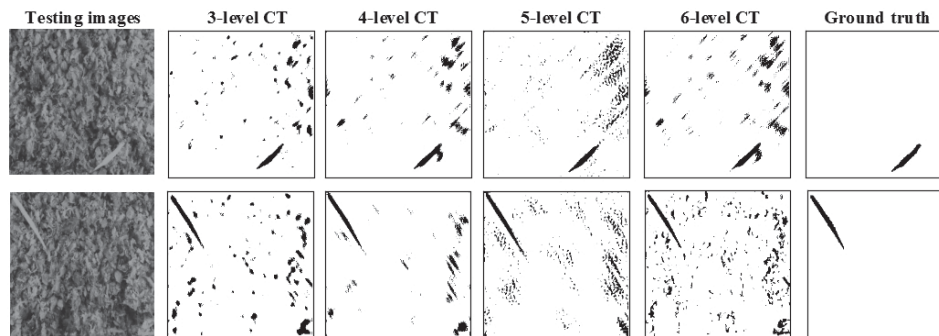


Figure 11: Two testing images and resulting outcomes of the proposed curvelet transform approach with various decomposition levels

### Parameter Selections

Choice of the key parameter, decomposition level, in the curvelet low-pass filtering operation will significantly influence the inspection performance of defects in the proposed method. To appraise the influence of altering diverse decomposition levels on rebuilt results, tests show the manifestation guides of inspection outcomes by changing decomposition levels from the range 3 to 6 pixels. Figure 11 shows two testing images and the corresponding resulting outcomes by using the suggested method with four decomposition levels. Table 1 presents the defect detection results for the four decomposition levels in three performance indices. The figures demonstrate that too little the number of decomposition level

(e.g. 3) cannot adequately separate defects from the fish floss surfaces and leads to some of incorrect alerts. However, too big the numbers of decomposition levels (e.g. 5 and 6) produce the diverse effect of the defects and causes many false warnings. The number of decomposition level 4 is more appropriate to underline defects in the curvelet low-pass filtering domain. Our trials on a variety of testing images have verified that decomposition level 4 is ordinarily appropriate for this defect inspection application.

In the procedure of defect segmentation, selecting a suitable manipulated parameter  $N$  (in Eq.(4)) leads to accurately differentiating defects from usual districts but an unsuitable manipulated parameter makes lots of mistakenly inspecting fish floss districts as defects. All trail

Table 1: Performance indices of four different curvelet transforms decomposition levels

Decomposition levels	False alarm rate $\alpha$ (%)	Defect inspection rate $1-\beta$ (%)	Correct classification rate CCR (%)
3 levels	1.95	81.18	94.98
4 levels	2.83	82.11	97.35
5 levels	3.78	85.42	95.20
6 levels	4.25	90.06	95.70

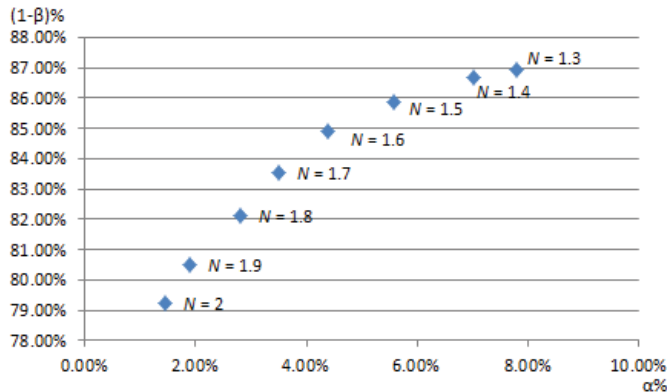


Figure 13: Various places of the two-paired guides ( $\alpha$ ,  $1-\beta$ ) for threshold values from scope  $1.3\sigma$  to  $2\sigma$  on the receiver operating characteristic plane

samples revealed in this research are originated in the  $\mu$  and  $\sigma$  from initial images, and the manipulated parameter  $N$  is assigned at various values. To assess the influence of changing various control values on the rebuilt results, tests show the manifestation guides of inspection outcomes by control values from the range 1.3 to 2.0. Figure 12 shows two testing images and the correspond-

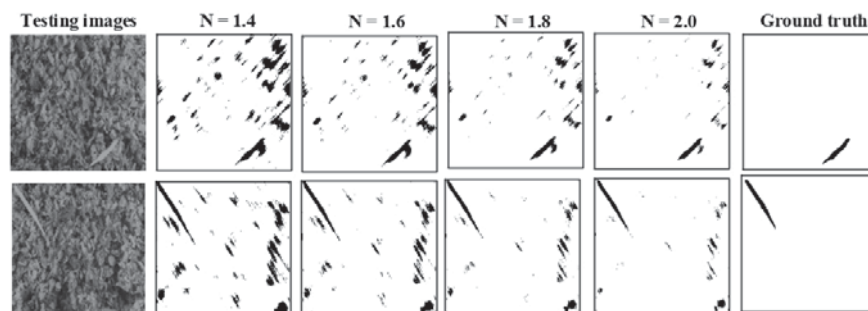


Figure 12: Two testing images and resulting outcomes of the proposed curvelet transform approach with various threshold values from scope  $1.4\sigma$  to  $2\sigma$

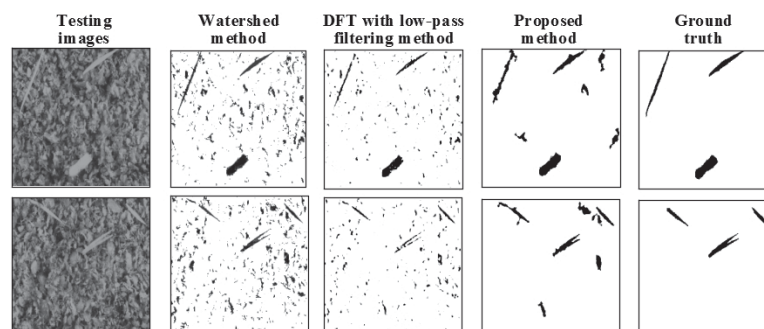


Figure 14: Detection outcomes of two testing images for defect inspection by watershed method, DFT filtering method, recommended method, and manual inspection

ing resulting outcomes by using the suggested method with threshold values from scope  $1.4\sigma$  to  $2\sigma$ . Figure 13 presents various places of the two-paired guides ( $\alpha$ ,  $1-\beta$ ) for the control values from scope  $1.3\sigma$  to  $2\sigma$  on the receiver operating characteristic plane [30]. The resulting outcomes and the curve indicate that smaller constant values  $N$  (e.g.  $1.3 \sim 1.7$ ) make strict controls and may lead to too many false alarms and bigger constant values (e.g.  $1.9 \sim 2.0$ ) make baggy controls and may cause some missing alarms. The number of constant value 1.8 is more appropriate to stress defects in the separations of defects from normal fish flosses. The trials on a variety of testing images have confirmed that control value 1.8 is ordinarily appropriate for this defect inspection application.

### Performance Evaluation

Two existing schemes usually applied to anomaly detection is contrast to the recommended approach to differentiate effects of fish bone inspection. To indicate the fault inspection outcomes of a testing image, Figure 14 demonstrates fractional outcomes of inspecting fish bones by the watershed method [31], the discrete Fourier transform (DFT) based low-pass filtering method [32], the recommended method, and the ground truth provided by inspectors, separately. The watershed method produces many erroneous judgments in false alarms and the DFT filtering method causes many of erroneous judgments in missing alarms on appearance fault inspection. The suggested method inspects most of the defects and produces less erroneous judgments. Therefore, the suggested technique surpasses the watershed method and DFT low-pass filtering method in the fish bone detection of fish floss with uneven surfaces.

Table 2: Summary table of differentiating effects by three defect detection methods

Detection schemes	Recall rate (%)	Precision rate (%)	F-score (%)	Accuracy rate (%)	Processing time (sec)
Watershed method	77.71	68.34	72.72	91.80	0.18
DFT low-pass filtering method	69.32	82.85	75.48	96.34	0.42
Suggested method	82.11	87.62	84.78	97.35	0.81

For more detailed comparisons of the three methods, the following performance indices, precision, recall, F-score and accuracy, are used to evaluate the individual methods. In this study, the precision index divides the regions of inspected actual defect districts by the regions of inspected defect districts to gain the positive predictive value. The recall index divides the regions of inspected actual defect districts by the regions of all actual defect districts to obtain the true positive rate. The F-score index is measuring the harmonic mean of the precision and the recall and provides a single score that balances both the concerns of precision and recall in one number. The accuracy index is the same as the correct classification rate.

Table 2 indicates the differentiating effects of defect detection consequences in the performed trials. A spatial domain skill and two frequency domain techniques are evaluated contrary to the consequences by practical examiners. The average defect inspection rates (Recall) of total trial samples by the three ways are, 77.71% by watershed method, 69.32% by DFT filtering method, and 82.11% by suggested method. Nevertheless, the two existing techniques have notably larger imprecision rates (1-Precision), 31.66% by watershed method, and 17.15% by DFT filtering method. Contrarily, the suggested scheme has a smaller imprecision rate 12.38%. The suggested method has a larger F-score, 84.78%, and a higher correct classification rate (Accuracy), 97.35%, than do the other skills utilized to defect detection of fish floss images. More concretely, the suggested approach has a larger defect inspection recall rate as well as has a smaller imprecision rate utilized to fish floss images having high uneven surfaces.

The average computation time for treating an image with 256 x 256 pixels is as follows: 0.18 seconds by watershed method, 0.42 seconds by DFT filtering method, and 0.81 seconds by recommended method. The mean processing time of the suggested scheme is nearly two times larger than that of the DFT filtering method yet it can be improved for actual fulfillment of an automatic optical detection system through hardware enhancement. The suggested approach conquers the problems of detecting defects in fish floss images with uneven exteriors and overbears in its capability of correctly discriminating defects from usual districts.

## CONCLUSION

This study presented a wrapping-based curvelet transform approach applied to developing an automatic optical inspection system for replacing human inspectors in fish floss inspection works. The proposed method conducts the low-pass energy filtering in frequency domain to remove the random patterns of background and delete the angle direction of background texture. Within the reconstructed image, the background random texture is attenuated and the defect areas are enhanced. Finally, the restored image can be easily segmented by an estimated threshold value into two categories namely dark defects, and white background. From the comparison studies, it is obvious that the proposed method well balances the trade-off between the recall rate (82.11%) and precision rate (87.62%), and reaches an F-score of 84.78%, outperforming the traditional defect detection techniques, the typical spatial domain skill and the Fourier based filtering approach, in inspection of dried fish floss. The prospective outcomes represent that curvelet transform could become known as a valid answer to texture analysis problems in future.

## ACKNOWLEDGEMENTS

This research was fractionally sponsored by the Ministry of Science and Technology, Taiwan, for the financial assistance through the Grant MOST 107-2221-E-324-016.

## REFERENCES

- Fitriya, W., Ekantari, N. (2019). Projective mapping and descriptive analysis of commercial fish floss in Yogyakarta Region. IOP Conference Series: Earth and Environmental Science, 370, 012069.
- Poonsri, T., Jafarzadeh, S., Ariffin, F., Ismail, N., Barati, Z., Latif, S., Muller, J. (2019). Improving the physicochemical and antioxidant properties of fish floss incorporated with waste cassava leaves. Journal of Chemical Health Risks, 9(1), 27-34.
- El-Mesery, H.S., Mao, H., Abomohra, A.E. (2019). Applications of non-destructive technologies for agricultural and food products quality inspection. Sensors, 19, 846.
- Lin, H.D., Chen, H.L. (2018). Automated visual fault inspection of optical elements using machine vision technologies. Journal of Applied Engineering Science, 16(4), 447-453.
- Chiu, Y.P., Lin, Y.K., Lin, H.D. (2020). Effective image models for inspecting profile flaws of car mirrors with applications. Journal of Applied Engineering Science, 18(1), 81-91.
- Gowen, A.A., Taghizadeh, M., O'Donnell, C.P. (2009). Identification of mushrooms subjected to freeze damage using hyperspectral imaging. Journal of Food Engineering, 93, 7-12.

7. Huang, W., Li, J., Wang, Q., Chen, L. (2015). Development of a multispectral imaging system for online detection of bruises on apples. *Journal of Food Engineering*, 146, 62-71.
8. Khoje, S.A., Bodhe, S.K., Adsul, A. (2013). Automated skin defect identification system for fruit grading based on discrete curvelet transform. *International Journal of Engineering and Technology*, 5(4), 3251-3256.
9. Chen, K., Qin, C. (2008). Segmentation of beef marbling based on vision threshold. *IEEE Xplore, Computers and Electronics in Agriculture*, 62, 223-230.
10. Brosnan, T., Sun, D.W. (2004). Improving quality inspection of food products by computer vision - a review. *Journal of Food Engineering*, 61, 3-16.
11. Andersen, K. (2003). X-ray techniques for quality assessment. In: Lutén, J.B., Oehlenschlaeger, J., Olafsdottir, G. (Eds.). *Quality of Fish from Catch to Consumer: Labelling, modelling and traceability*. Wageningen Academic Publishers, 283-286.
12. Han, Y., Shi, P. (2007). An efficient approach for fish bone detection based on image preprocessing and particle swarm clustering. *Communications in Computer and Information Science*, 2, 940-948.
13. Thielemann, J., Kirkhus, T., Kavli, T., Schumann-Olsen, Haugland, O., Westavik, H. (2007). System for estimation of pin bone positions in pre-rigor salmon. In: *Lecture Notes in Computer Science. Advanced Concepts for Intelligent Vision Systems (ACIVS2007)*, 4678, 888-896.
14. Sivertsen, A.H., Chu, C.K., Wang, L.C., Godtliebsen, F., Heia, K., Nilsen, H. (2009). Ridge detection with application to automatic fish fillet inspection. *Journal of Food Engineering*, 90, 317-324.
15. Mery, D., Lillo, I., Loebel, H., Rizzo, V., Soto, A., Cipriano, A., Aguilera, J.M. (2011). Automated fish bone detection using X-ray imaging. *Journal of Food Engineering*, 105, 485-492.
16. Rerkratn, A., Kaewpoonsuk, A. (2014). System development for quality evaluation of fish fillet using image processing. *Proceedings of the 2014 International Conference on Computer, Communications and Information Technology*, 196-199.
17. Boubchir, L., Fadili, J.M. (2005). Multivariate statistical modeling of images with the curvelet transform. *IEEE Xplore*, 1581046, 747-750.
18. Jiang, T., Zhao, X. (1999). Research and application of image denoising method based on curvelet transform. *The International Archives of the Photogrammetry*, 62, 363-368.
19. Zhang, Y., Li, T., Li, Q. (2013). Defect detection for tire laser shearography image using curvelet transform based edge detector. *Optics & Laser Technology*, 47, 64-71.
20. Li, L., Zhang, X., Zhang, H., He, X., Xu, M. (2015). Feature extraction of non-stochastic surfaces using curvelets. *Precision Engineering*, 39, 212-219.
21. Kalaivani, M., Jeyalakshmi, M.S., Aparna, V. (2012). Extraction of retinal blood vessels using curvelet transform and Kirsch's templates. *International Journal of Emerging Technology and Advanced Engineering*, 2, 360-363.
22. Mandal, T., Wu, Q.M.J. (2008). Face recognition using curvelet based PCA. *2008 19th International Conference on Pattern Recognition*, 1-4.
23. Khosrow-Pour, M. (2014). *Encyclopedia of Information Science and Technology*, 3rd Ed., IGI Global.
24. Salau, A.O., Jain, S. (2020). Computational modeling and experimental analysis for the diagnosis of cell survival/death for Akt protein. *Journal of Genetic Engineering and Biotechnology*, 18(11), 1-10.
25. Candes, E.J., Donoho, D.L. (2000). Curvelets: A surprisingly effective non-adaptive representation for objects with edges. in *Curve and Surface Fitting: Saint-Malo Proceedings*, Cohen, A., Merrien, J.-L., Schumaker, L.L., Eds. Nashville, TN: Vanderbilt Univ. Press, 105-120.
26. Cand, E.J., Donoho, D.L. (2004). New tight frames of curvelets and optimal representations of objects with C2 singularities. *Department of Statistics, Communications on Pure and Applied Mathematics*, 57(2), 219-266.
27. Cand, E.J., Demanet, L., Donoho, D., Ying, L. (2006). Fast discrete curvelet transforms. *Multiscale Modeling & Simulation*, 5(3), 861-899.
28. Salau, A.O., Jain, S. (2019). Feature extraction: a survey of the types, techniques, applications. *Proceedings of 2019 International Conference on Signal Processing and Communication (ICSC)*, 158-164.
29. Alhanjouri, M.A. (2011). Curvelet and waveatom transforms based feature extraction for face detection. *Journal of al-Aqsa University: Series of Natural Sciences*, 15(1), 41-66.
30. Montgomery, D.C., Runger, G.C. (2007). *Applied Statistics and Probability for Engineers*. 4th Edition, John Wiley & Sons, New Jersey, USA.
31. Couprie, M., Bertrand, G. (1997). Topological Gray-scale Watershed Transformation. *SPIE Vision Geometry VI Proceedings*, 3168, 136-146.
32. Lin, H.D., Tsai, H.H. (2012). Automated quality inspection of surface defects on touch panels. *Journal of the Chinese Institute of Industrial Engineers*, 29(5), 291-302.

*Paper submitted: 21.06.2020.*

*Paper accepted: 03.08.2020.*

*This is an open access article distributed under the CC BY 4.0 terms and conditions.*